

# Detailed study of the phase transition in $[\text{Ni}(\text{H}_2\text{O})_6](\text{NO}_3)_2 \cdot (15\text{-crown-5}) \cdot \text{H}_2\text{O}$ and analysis in terms of mean-field theory

Maxime A. Siegler,<sup>a</sup> Sean Parkin,<sup>a</sup> Ross J. Angel<sup>b</sup> and Carolyn Pratt Brock<sup>a\*</sup>

<sup>a</sup>Department of Chemistry, University of Kentucky, Lexington, Kentucky 40506-0055, USA, and <sup>b</sup>Crystallography Laboratory, Department of Geosciences, Virginia Tech, Blacksburg, Virginia 24060, USA

Correspondence e-mail: cpbrock@uky.edu

Received 19 October 2010

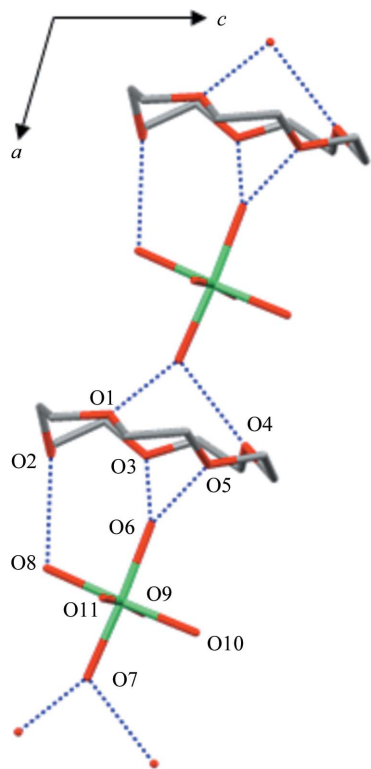
Accepted 12 February 2011

The transition between 190 and 200 K in  $[\text{Ni}(\text{H}_2\text{O})_6](\text{NO}_3)_2 \cdot (15\text{-crown-5}) \cdot \text{H}_2\text{O}$  has been followed by determining the structure at 22 temperatures in the range 90–273 K. The structural change is a zone-boundary transition with a critical point at  $(\frac{1}{2}, 0, \frac{1}{2})$  in the Brillouin zone of the high-temperature phase; both phases have space-group symmetry  $P2_1$  but the volume of the unit cell is halved when a crystal is heated through the transition. The only obvious disorder in the high-temperature phase is of the lattice water molecule, which occupies two sites; some disorder persists below the transition. The greatest changes in the structure below the transition are the rotations of one of the two 15-crown-5 molecules and of one of the two nitrate ions; above the transition the two molecules are related by symmetry as are the two ions. Below the transition these two rotation angles evolve linearly with one another, and can thus be associated with a single order parameter that describes the structural evolution. The evolution of the spontaneous strain arising from the transition does not, however, follow the same evolution as the structural order parameter. This observation indicates that the transition cannot be described in terms of a Landau-type expansion that is characterized by a single order parameter, perhaps because the potential-energy surface for this essentially molecular crystal is more complicated than for the inorganic and framework structures in which such simple behaviour is observed.

## 1. Introduction

Crystals of the first polymorph of  $[\text{Ni}(\text{H}_2\text{O})_6](\text{NO}_3)_2 \cdot (15\text{-crown-5}) \cdot \text{H}_2\text{O}$  (hereafter, NiW6-W) were obtained while working out how to make  $[\text{Ni}(\text{H}_2\text{O})_2(15\text{-crown-5})](\text{NO}_3)_2$  (see Siegler *et al.*, 2008). The important motif in these crystals is a hydrogen-bonded chain (Siegler *et al.*, 2010) in which  $[\text{Ni}(\text{H}_2\text{O})_6]^{2+}$  cations and 15-crown-5 molecules (hereafter, 15C5) alternate (see Fig. 1). The cations in the chains are crosslinked by hydrogen bonds (see Fig. 2).

The structures of NiW6-W at 90 K (Siegler *et al.*, 2008) and at room temperature are slightly different; the crystals undergo a nondestructive phase transition during cooling. The volume of the room-temperature  $P2_1$ ,  $Z' = 1$  cell is doubled below the transition but the point-group symmetry remains the same (see Fig. 3). Comparisons of the structures at 295 and 90 K show that the most obvious structural change is a small rotation of one half of the 15C5 molecules around an axis approximately perpendicular to their best-fit molecular plane (see Fig. 3) so that in the low-temperature phase rotated and unchanged 15C5 rings alternate along *c*. Such a rotation would be consistent with a simple displacive mechanism for the

**Figure 1**

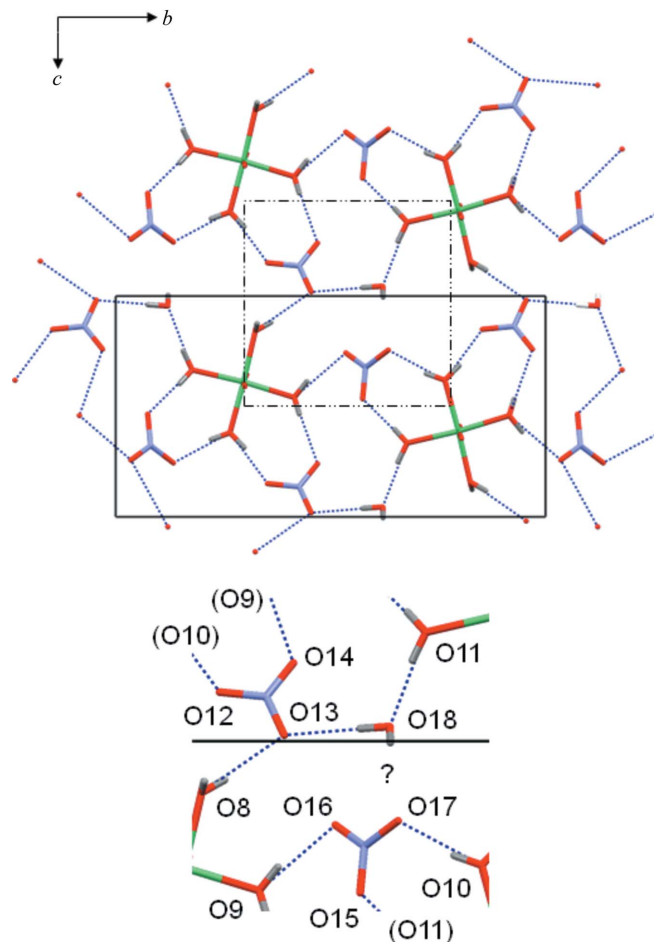
Drawing showing part of the hydrogen-bonded chain of  $[\text{Ni}(\text{H}_2\text{O})_6]^{2+}$  cations and 15-crown-5 molecules that extends along the **a** axis. H atoms have been omitted in this and most subsequent drawings. The **b** axis points into the plane of the paper. In the high-temperature phase, which is shown, the two cations and the two crown molecules are related by the translation along **a**. The numbering scheme for the O atoms in the chain is shown. In the ring the bonded atoms are O1–C1–C2–O2–C3–C4–...–C10–O1. In the low-temperature structure the two independent sets of atoms are distinguished by adding **\_1** and **\_2** to the atom names.

transition in the sense that it does not require changes in the molecular conformation or the packing.<sup>1</sup> Since diffraction data can be collected so quickly with a CCD detector and since the phase transition in this compound is nondestructive and occurs at a convenient temperature (*ca* 200 K) we decided to make a detailed study of the change in the structure with *T*; we hoped to be able to identify the reason for the transition. The transition between the high- and low-temperature phases was also followed by DSC (differential scanning calorimetry).

In a Feature Article in this journal Herbstein (2006) pointed out the lack of information ‘about changes in crystal structure, including changes in cell dimensions, as the system passes through the transition’. A search of version 5.31 (November 2009) and the February 2010 update of the Cambridge Structural Database (CSD: Allen, 2002) for studies in which structures were determined at least four temperatures below and four temperatures above a transition gave only 12 hits<sup>2</sup>

<sup>1</sup> In standard terminology the term ‘displacive’ does not imply a distinction between static or dynamic displacements.

<sup>2</sup> A search of the CSD for structures that include ‘phase transition’ in a text string turned up *ca* 3000 refcode families. The 45 families in that list that included at least eight entries were then examined individually with reference to the original papers.

**Figure 2**

Drawings showing the hydrogen-bond pattern in the plane of the **b** and **c** axes; the 15-crown-5 molecules are not shown because they do not take part in this pattern. The lower image is an enlargement that corresponds to the approximate square that is marked with broken lines on the upper image. The atom-numbering scheme is given. Atom N1 is bonded to O12 and atom N2 to O15. The unit cell shown is for the high-temperature structure; in the low-temperature structure the **c** axis is twice as long and the two independent sets of atoms, which are related by a pseudotranslation along **c**, are distinguished by adding **\_1** and **\_2** to the atom names. No hydrogen bond from O18 to O16 and/or O17 is marked because of the uncertainty about its position. Only the major position of the disordered water molecule is shown, but the two sites are close together (see Fig. 3).

(see Table 1).<sup>3</sup> The transitions in six of the 12 involve spin changes and so are structurally distinct from the transition described in this work, although the underlying physics of the evolution of the structures below the phase transition may be the same or similar. This study aimed to provide detailed information about a purely structural transition in a crystal that is essentially molecular even though it contains charged species.

We discovered that while the largest molecular motions associated with the transition in NiW6-W could be identified, detailed analyses generated as many questions as answers. All the structural changes can be characterized with the tools developed in the study of structural phase transitions in

<sup>3</sup> The study of David *et al.* (2006) of  $\text{S}_8$  at 37 temperatures should also be mentioned even though coordinates are given in the associated CIF for the 100 K structure only.

inorganic materials, but the characteristics of the transition cannot be described in terms of the evolution of a single order parameter. Mean-field theory has been very successful in describing phase transitions in inorganic systems, especially perovskites (Carpenter *et al.*, 2001; Howard & Stokes, 2005; Carpenter, 2007), but its general applicability to molecular systems, which are usually of lower symmetry and in which the forces act over much shorter distances, remains uncertain.

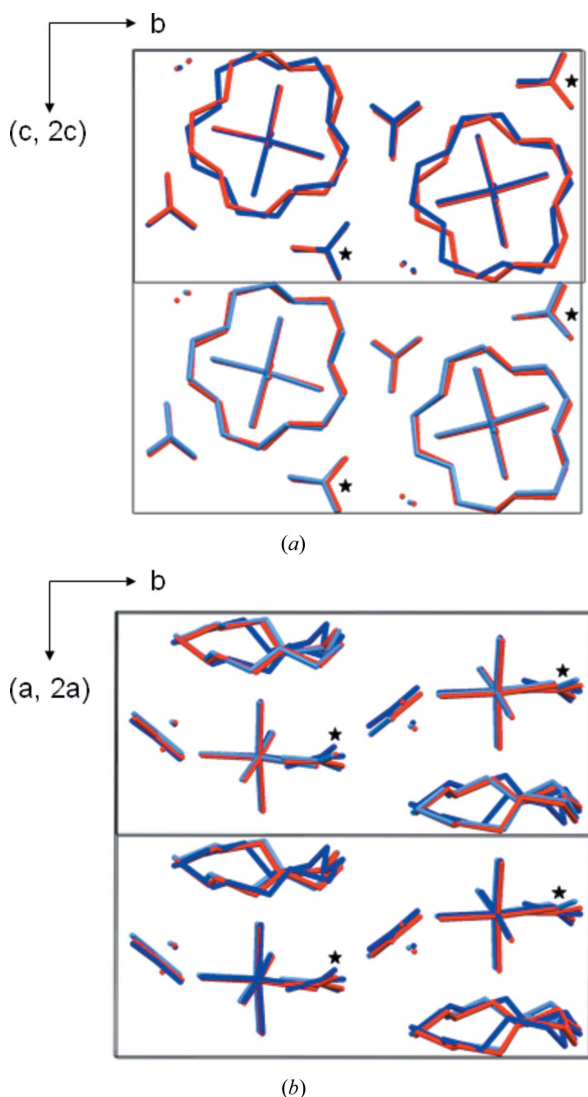


**Figure 3**  
Overlays of the structures determined at 160 K [darker blue for the first independent formula unit ( $z < 0.5$ ) and lighter blue for the second ( $z > 0.5$ ) and at 210 K (red;  $0 < z < 2$ ). The pictures show how similar the structures are except for the orientation of the first 15-crown-5 ring. The displacements of the nitrate ions containing N1\_1, which are marked with a star and which are superimposed on the nitrate ions containing N1\_2, are less obvious. (a) View along **a**; projection limited to  $0 < x < \frac{1}{2}$  because rings 1 and 2 alternate along **a**. The axis **b** = **b<sub>HT</sub>** = **b<sub>LT</sub>** is in the plane of the drawing but **c** = **c<sub>HT</sub>** and **2c** = **c<sub>LT</sub>** points out of the plane. (b) View along **c**. The structure at 210 K was chosen because 210 K is the the lowest temperature in the set that is clearly above the phase transition. The axis **b** = **b<sub>HT</sub>** = **b<sub>LT</sub>** is in the plane of the drawing but **a** = **a<sub>HT</sub>** and **2a** = **a<sub>LT</sub>** are behind the plane. An overlay of the structures at 190 and 210 K is uninformative because the two structures are so similar.

## 2. Terminology

As used by many physicists the term ‘structural phase transition’ has a very specific definition based in symmetry. That is, the symmetry of the low-symmetry phase is a subgroup of the symmetry of the high-symmetry phase, and the structural changes can be described in terms of modes with symmetries given by the irreducible representations of the parent space group. These modes have recently become known as ‘symmetry-adapted modes’ (Perez-Mato *et al.*, 2010). In this sense there is no distinction between a ‘structural’ phase transition that arises from molecular displacements, and one that arises from ordering of electrons or of magnetic moments. All can be ‘structural’ phase transitions provided the relationship between the structures and symmetries of the phases involved meets the requirements stated above. Clearly, as a consequence the description ‘structural phase transition’ says nothing about the mechanism of the transition. Neither does it say whether the thermodynamics of the transition is continuous or first order. In inorganic materials the same transition can change character from first order to continuous with just a change in composition (*e.g.* Arlt & Angel, 2000; Tribaudino *et al.*, 2002, 2003) or state of atomic order (Angel, 1992) without any change in mechanism.

As a consequence, the concept of a structural phase transition, which is defined by the symmetry, and of a structural change, which is defined by changes of atomic coordinates, is independent of mean-field theories, which say something about the thermodynamics of the transition.

## 3. Experimental

### 3.1. Synthesis and morphology

Pale green crystals were grown by evaporation at room temperature from concentrated acetone solutions equimolar in  $\text{Ni}(\text{NO}_3)_2 \cdot 6\text{H}_2\text{O}$  and 15C5. We saw no evidence under a light microscope or in the DSC curves of contamination of monohydrate samples by the dihydrate or by the second polymorph of the monohydrate (see Siegler *et al.*, 2008; Siegler, 2007). The crystals were laths elongated along **a**, *i.e.* the direction of the hydrogen-bonded chains (see Fig. 1).

### 3.2. Differential scanning calorimetry (DSC)

The thermal behavior of the compound was investigated using the DSC 822° apparatus from METTLER TOLEDO under the control of the software STARe (Version 8.10). The DSC samples were prepared from fine powders. The sample (several mg in a pierced Al pan) was cooled at a rate of  $10 \text{ K min}^{-1}$  from room temperature to 173 K, held at that temperature for a few minutes and then reheated at the same rate. Part of a typical DSC trace is shown in Fig. 4.<sup>4</sup>

<sup>4</sup> The DSC results are evidence that the sample was not contaminated by the dihydrate (of  $[\text{Ni}(\text{H}_2\text{O})_6](\text{NO}_3)_2 \cdot (15\text{-crown-5}) \cdot 2\text{H}_2\text{O}$ ). The dihydrate compound has phase transitions at 288, 234 and 195 K (Siegler, 2007). The first and last of these have substantially larger  $\Delta_{\text{trans}}H^\circ$  values than the transition in the monohydrate. The transition at 195 K of the dihydrate has obvious hysteresis; the transition temperatures for cooling and heating vary by *ca* 10 K. None of these features is apparent in the curves reported here.

**Table 1**

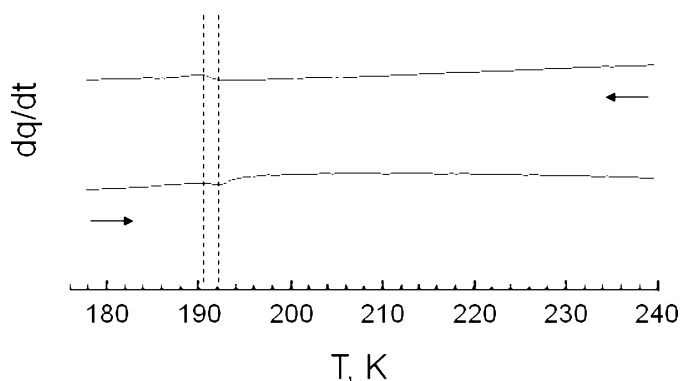
Multi-temperature studies of phase transitions in molecular systems.

Studies listed have coordinates in the CSD for at least four temperatures each above and below a transition. The numbers of structures below, 'during' (in parentheses) and above the transition are listed. It is often not possible to decide with certainty how a structure determined near a transition should be described, especially if there is significant hysteresis, so the structure counts shown below are not definitive. The description 'same unit cell' indicates that the cell constants do not change across the transition by more than a few per cent.

| Refcode family and numbers     | Reference  | Chemical formula   | Symmetry change (given for decreasing $T$ )  | Transition type (given for decreasing $T$ )  | $T_{trans}$ (K); structure count               |
|--------------------------------|--|--|--|--|--|
| BARBAD(02-15)<br>BOQCUF(01-10) | Nichol & Clegg (2005)<br>Minkov <i>et al.</i> (2009) | $C_4H_4N_2O_3 \cdot 2H_2O$<br>$C_3H_7NO_2S$                          | $Pmnb \rightarrow P2_1/n$<br>$P2_1/a$ in both phases;<br>same unit cell                | Small packing changes<br>Rotation of $CH_2SH$<br>group around the C—<br>C bond                       | 215–217 [6, (3), 5]<br>205–320 [5, 5]          |
| CEDBUJ(11-24)                  | Casati <i>et al.</i> (2009)                          | $C_{42}H_{30}Co_2O_6P_2$   | $R\bar{3}$ in both phases but $c$<br>is doubled  | Change of conformation<br>from staggered to<br>eclipsed  | 119–124 [6, 8]                                 |
| EKAXOD(00-16)                  | Hashizume <i>et al.</i> (2003)                       | $C_9H_{18}N_2O_2$  | $P\bar{1}$ in both phases; same<br>unit cell   | Shear of layers and<br>ordering of<br>$CH_2CHMe_2$ group   | 363–368 [11, (3), 3]                           |
| FEPICC(22-37)                  | Chernyshov <i>et al.</i> (2003)                      | $[C_{18}H_{24}FeN_6]Cl_2 \cdot C_2H_6O$                              | $B2_1/c$ in high- and low-<br>temperature phases;<br>$P2_1/c$ in intermediate<br>phase | Spin-crossover transi-<br>tion with intermediate<br>phase  | $\sim 114$ ; $\sim 124$ [3, (2), 5,<br>(3), 6] |
| GOGJAN(09-19)                  | Casati <i>et al.</i> (2009)                          | $C_{42}H_{30}Co_2O_6As_2$  | $R\bar{3}$ in both phases but $c$<br>is doubled  | Small conformational<br>change (change in<br>dihedral angle<br>describing staggered<br>conformation) | 170–210 [5, 6]                                 |
| HAYFOC(01-16)                  | Goeta <i>et al.</i> (2007)                           | $[C_{20}H_{30}Cr_2P_5][SbF_6]$                                       | $Fddd \rightarrow I2/a$ ; lattice is<br>maintained                                     | Spin-crossover transi-<br>tion in $Cr_2$ with<br>ordering of $P_5$ rings                             | $\sim 19$ ; $\sim 160$ [1, 8, 7]               |
| IBIXAT(01-21)                  | Törnroos <i>et al.</i> (2006)                        | $[C_{18}H_{24}FeN_6]Cl_2 \cdot C_3H_8O$                              | $B2_1/c \rightarrow P2_1/c \rightarrow B21/c$ ;<br>same unit cell                      | Spin-crossover transi-<br>tion with solvent<br>ordering  | [21 total]                                     |
| NIQFUP(00-11)                  | Seredyuk <i>et al.</i> (2007)                        | $[C_{27}H_{33}FeN_7](ClO_4)_2$                                       | $P2_1/c$ in both phases;<br>same unit cell   | Spin-crossover transi-<br>tion with small<br>changes in packing                                      | $\sim 233$ [6, 1, 6]                           |
| SOHSUE(00-10)                  | Ovcharenko <i>et al.</i> (2008)                      | $[C_{48}H_{50}Cu_2F_{24} \cdot$<br>$N_8O_{12}]_n \cdot n(C_6H_{14})$ | $P\bar{1}$ in both phases but $a$<br>is doubled  | Spin-crossover transi-<br>tion with solvent<br>ordering  | $\sim 161$ [4, (2), 5]                         |
| UBUQIR(00, 02, 04-14)          | Haddon <i>et al.</i> (2008)                          | $C_{30}H_{24}BN_2O_2$  | $P2_1/c$ in both phases;<br>same unit cell   | Magnetic transition  | $\sim 140$ [7, (1), 5]                         |
| WOLYUR(01-15)                  | Budzianowski <i>et al.</i><br>(2008)                 | $C_6H_{13}N_2^+ \cdot BF_4^-$  | $Pm2_1n \rightarrow Pb2_1a$ with<br>doubling of $a$                                    | Ordering of anions,<br>cations   | 153 [7, 8]                                     |
| ROLBOK( <i>nn-mm</i> )         | This work  | $[H_{12}NiO_6](NO_3)_2 \cdot C_{10}H_{20}O_5 \cdot H_2O$             | $P2_1 \rightarrow B2_1$ with doubling<br>of $a, c$                                     | Small packing changes  | 195–200 [13, (2), 7]                           |

### 3.3. Structure determinations

All X-ray data to  $\sin \theta/\lambda = 0.65 \text{ \AA}^{-1}$  ( $27.5^\circ$  for Mo  $K\alpha$  radiation) were collected with a Nonius KappaCCD diffractometer equipped with a CRYOCOOL-LN2 low-temperature

**Figure 4**

DSC trace during one cooling/heating cycle of a typical sample of  $[Ni(H_2O)_6](NO_3)_2 \cdot (15\text{-crown-5}) \cdot H_2O$ .

system (CRYO Industries of America, Manchester, NH). Our calibrations of the CRYOCOOL-LN2 system using  $N_2(l)$ , the phase transition in  $KH_2PO_4(s)$  near 122 K and an  $H_2O(s)/H_2O(l)$  bath indicate that the temperature precision is at least 0.2 K and the accuracy no worse than 0.5 K. In most cases, and at all temperatures near the phase transition, the data in the unintegrated frames were transformed (Nonius, 2000) to show slices  $nkl$ ,  $hnl$  and  $hkn$ ,  $n = 0-3$ , of the reciprocal lattice (see, e.g., Fig. 5).

Data were measured at 90 K (Siegler *et al.*, 2008) and then later at 295 K (reported here) for a separate crystal. Data were measured for a third crystal, which was initially flash-cooled to 90 K, at 22 temperatures in the range  $90 \rightarrow 273$  K. Data in this temperature sequence were measured at heating intervals of 10 K except in the region 170–200 K, where the interval was 5 K, and 220–233 K, where the interval was 13 K. Data collection took 2.2 h at each temperature and was not started until at least 30 min after the temperature had been changed. It took less than a week to collect the 22 sets of data. Much later, data were collected for a fourth crystal that was cooled

quickly to 250 K, and then cooled slowly (no more than 2 K in 5 min) to 100 K. Full data sets for this fourth crystal were collected at 250, 185, 170, 150 and 100 K.

The conventional space group  $P2_1$  of the low-temperature structure was changed to  $B2_1$  so that the directions of the axes **a** and **c**, as well as **b**, would be the same in the two cells. When crystals are cooled through the transition the lengths *a* and *c* are both doubled, but the size of the asymmetric unit increases by only a factor of two because of the added cell centering. The transformation matrix that relates the non-standard and conventional low-temperature cells is given by

$$\mathbf{a}(B2_1) = (1\ 0\ 1/0\ -10/10\ -1)\mathbf{a}(P2_1). \quad (1)$$

The cell constants of the  $P2_1$  cell for the third crystal at 90 K are  $a = 10.220$  (1),  $b = 16.514$  (2),  $c = 13.644$  (2) Å, and  $= 95.96$  (1)°.<sup>5</sup>

Data collected at 210 K and above were integrated using the high-temperature unit cell. Data collected at 195 and 200 K were integrated using the larger low-temperature cell with **a** and **c** doubled, but the number of *hkl*, *h* or *l* odd, reflections having  $I > 2\sigma(I)$  was so small, especially at 200 K (see Fig. 5), that the structures at 195 and 200 K had to be refined with the high-temperature symmetry and unit cell.

Both phases were refined as ordered except for the lattice water molecule. In the high-temperature phase the one independent lattice water molecule (O18) is disordered. In the low-temperature  $B2_1$  phase one of the two independent lattice water molecules (O18\_2) was treated as ordered, but it has a rather large displacement ellipsoid [ $U_{eq}$  0.042 (1)–0.106 (3) for 90–190 K compared with 0.031 (2)–0.048 (2) Å<sup>2</sup> for O18\_1]. At 90 K there is a peak in the final difference-Fourier map near O18\_2, but its height is only 0.37 e Å<sup>-3</sup>. Occupancy factors for the major positions are shown in Fig. 6.

All refinements were performed with the same settings, constraints and restraints. The atom-numbering schemes (see Figs. 1 and 2) are the same as in Siegler *et al.* (2008). During the final refinements the H atoms of the 15C5 ligands were placed at calculated positions [instruction AFIX 23 in *SHELXL97* (Sheldrick, 2008)] with isotropic displacement parameters having values  $1.2 \times U_{eq}$  of the attached C atom. The H atoms of coordinated waters were restrained such that the O–H distances and H–O–H angles would have values within accepted ranges [ $d(\text{O–H}) = 0.82\text{--}0.84$  Å;  $d(\text{H} \cdots \text{H}) \simeq 1.30$  Å so that  $\text{H–O–H} \simeq 104.5^\circ$ ]. Isotropic displacement

<sup>5</sup> Symmetry operations for  $B2_1$ :  $x, y, z$ ;  $-x, y + \frac{1}{2}, -z$ ;  $x + \frac{1}{2}, y, z + \frac{1}{2}$ ;  $-x + \frac{1}{2}, y + \frac{1}{2}, -z + \frac{1}{2}$ . Very late in this project we realised that the relationship between the phases might have been simpler to understand if we had used the conventional  $P2_1$  cell for the low-temperature phase. The most closely related cell for the high-temperature phase would then have the space group  $B2_1$  and the same dimensions as the cell for the low-temperature phase; the transition with heating that halves the size of the asymmetric unit ( $Z' = 2 \rightarrow Z' = 1$ ) would then be described as  $P2_1 \rightarrow B2_1$  ( $Z = 4 \rightarrow Z = 4$ ) rather than as  $B2_1 \rightarrow P2_1$  ( $Z = 8 \rightarrow Z = 2$ ). The principal axes of the thermal expansion tensor, however, are much more closely aligned with the  $\mathbf{a}_{\text{HT}}$  and the  $\mathbf{c}_{\text{LT}} = 2\mathbf{c}_{\text{HT}}$  axes used here than they are with the  $[1\ 0\ 1]$  and  $[-1\ 0\ 1]$  directions in those cells that would become the **a** and **c** axes for the other cell choice. A diagram showing the relationships of the two pairs of unit cells is given with the supplementary material.

parameters for the water H atoms were  $1.5 \times U_{eq}$  of the attached O atom.

The H-atom positions for the uncoordinated water molecule with the lower occupancy factor are roughly the same as for the molecule with the higher occupancy factor; the H atoms for the major component were therefore included at full occupancy. All attempts to locate separate H-atom positions for the minor component were unsuccessful.

All structures were determined to a similar precision. All *R* factors for reflections with  $I > 2\sigma(I)$  are  $< 0.050$ . All weighted *R* factors (all reflections) are  $\leq 0.106$  except at  $T = 190$  K (*i.e.* just below the phase transition but structure refined in the high-temperature cell), where  $wR_{\text{all}}$  is 0.147.

Values of the Flack parameter (Flack, 1983; Flack & Bernardinelli, 2000) for the first multi-*T* series were estimated by *SHELXL97* to vary from 0.066 to 0.103 with uncertainties in the range 0.009–0.013. No model for racemic twinning was included in the refinement because the Flack parameters are so small, but we concede the possibility of a small amount of the inverted structure. For the separate crystal studied at

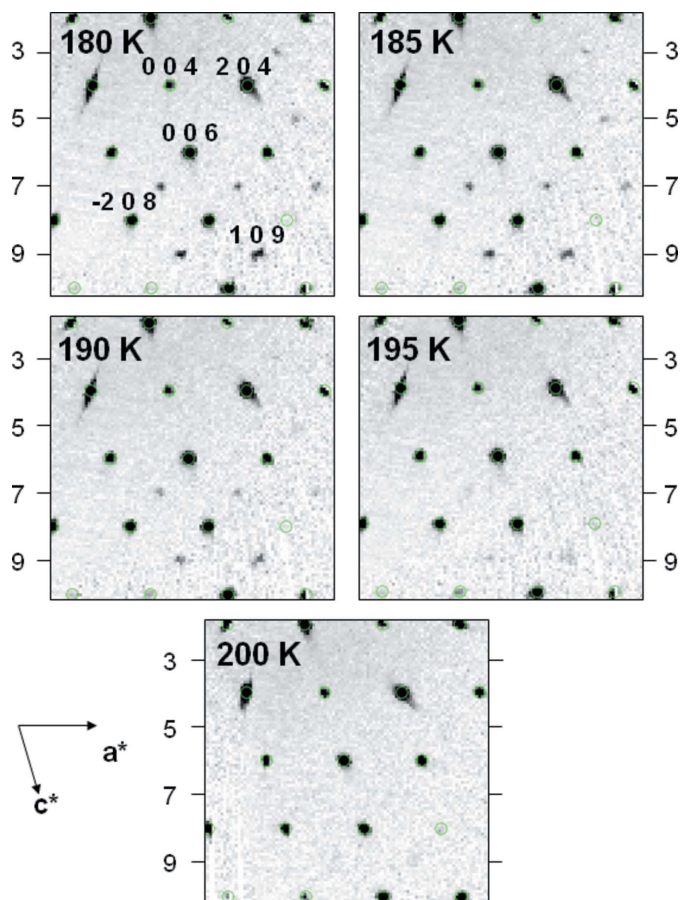


**Figure 5** One part of the *h0l* reciprocal-lattice slice as a function of temperature in the region of the phase transition. Some of the indices are shown. The rows having *l* odd are marked with tick marks along the sides of the drawings. The strongest superstructure reflections in these images have *l* = 7 and 9. Calculated positions for the *l* even reflections are marked by green circles that are light gray in the printed version of the journal. The *l* odd reflections are not marked.

**Table 2**

Experimental details for some NiW6-W structures near the phase transition.

For all structures:  $C_{10}H_{20}O_5 \cdot H_{12}NiO_6^{2+} \cdot 2NO_3^- \cdot H_2O$ ,  $M_r = 529.10$ . Experiments were carried out with Mo  $K\alpha$  radiation using a Nonius KappaCCD diffractometer. Absorption was corrected for by multi-scan methods, *SCALEPACK* (Otwinowski & Minor, 2006). H atoms were treated by a mixture of independent and constrained refinement. The absolute structure was obtained using Flack (1983).

|  | 150 K                              | 170 K                              | 180 K                              | 190 K                              | 210 K                            |
|--|------------------------------------|------------------------------------|------------------------------------|------------------------------------|----------------------------------|
| Crystal data   |                                    |                                    |                                    |                                    |                                  |
| Crystal system, space group  | Monoclinic, $B2_1$                 | Monoclinic, $B2_1$                 | Monoclinic, $B2_1$                 | Monoclinic, $B2_1$                 | Monoclinic, $P2_1$               |
| $a, b, c$ (Å)  | 16.222 (2), 16.571 (2), 17.882 (2) | 16.238 (2), 16.598 (2), 17.878 (2) | 16.246 (2), 16.618 (2), 17.870 (2) | 16.254 (2), 16.644 (2), 17.860 (2) | 8.134 (2), 16.675 (4), 8.926 (2) |
| $\beta$ (°)  | 106.34 (1)                         | 106.28 (1)                         | 106.24 (1)                         | 106.17 (1)                         | 106.09 (1)                       |
| $V$ (Å <sup>3</sup> )  | 4612.8 (9)                         | 4625.2 (10)                        | 4632.0 (10)                        | 4640.5 (10)                        | 1163.2 (5)                       |
| $Z$  | 8                                  | 8                                  | 8                                  | 8                                  | 2                                |
| $\mu$ (mm <sup>-1</sup> )  | 0.92                               | 0.92                               | 0.92                               | 0.92                               | 0.92                             |
| Crystal size (mm)  | 0.35 × 0.15 × 0.15                 | 0.35 × 0.15 × 0.15                 | 0.35 × 0.15 × 0.15                 | 0.35 × 0.15 × 0.15                 | 0.35 × 0.15 × 0.15               |
| Data collection  |                                    |                                    |                                    |                                    |                                  |
| $T_{min}, T_{max}$   | 0.738, 0.874                       | 0.739, 0.874                       | 0.739, 0.874                       | 0.739, 0.875                       | 0.740, 0.875                     |
| No. of measured, independent and observed [ $I > 2\sigma(I)$ ] reflections | 33 272, 10 584, 6204               | 33 222, 10 594, 5808               | 33 266, 10 619, 5539               | 16 694, 10 597, 4887               | 16 769, 5345, 4025               |
| $R_{int}$  | 0.071                              | 0.073                              | 0.074                              | 0.056                              | 0.057                            |
| Refinement   |                                    |                                    |                                    |                                    |                                  |
| $R[F^2 > 2\sigma(F^2)], wR(F^2), S$  | 0.044, 0.100, 0.99                 | 0.044, 0.102, 0.99                 | 0.045, 0.106, 0.97                 | 0.050, 0.147, 1.02                 | 0.042, 0.093, 1.03               |
| No. of reflections   | 10 584                             | 10 594                             | 10 619                             | 10 597                             | 5345                             |
| No. of parameters  | 648                                | 648                                | 648                                | 648                                | 327                              |
| No. of restraints  | 43                                 | 43                                 | 43                                 | 43                                 | 24                               |
| $\Delta\rho_{max}, \Delta\rho_{min}$ (e Å <sup>-3</sup> )                  | 0.81, -0.41                        | 0.75, -0.44                        | 0.88, -0.38                        | 1.02, -0.77                        | 0.92, -0.34                      |
| Flack parameter  | 0.068 (10)                         | 0.076 (10)                         | 0.082 (10)                         | 0.082 (13)                         | 0.089 (12)                       |

Computer programs used: *COLLECT* (Nonius, 2000), *SCALEPACK*, *DENZO-SMN* (Otwinowski & Minor, 2006), *SHELXS97*, *SHELXL97* (Sheldrick, 2008), *Mercury* (Macrae *et al.*, 2008), and local procedures.

295 K the value of the Flack parameter is  $-0.013$  (11). For the fourth crystal, which was studied at decreasing temperatures, the absolute value of the estimated Flack parameter was never larger than 0.007.

Information about five of the structure determinations carried out near the phase transition during the heating

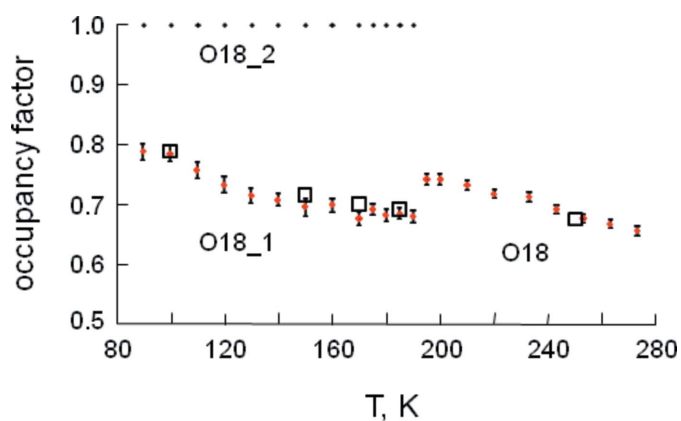


**Figure 6**

Variation with temperature of the occupancy factors for the O atoms of the lattice water molecules. The error bars, which are shown for the 22 structures of the heating sequence, extend one standard uncertainty above and one below the data points. There are no error bars for the occupancy of the atom O18\_2 because it was treated as ordered. Values for the five structures of the cooling sequence are shown as open squares.

sequence is shown in Table 2; full details of the other 17 + 5 determinations of the two temperature sequences are given in the supplementary material<sup>6</sup> as are details of the separate determination at 295 K. The estimated errors in the unit cell constants were obtained by multiplying the values given by the software by a factor of 3 for the cell constants and a factor of 15 for the cell angles. These factors were used in order to take into account the variation in the unit-cell constants from one crystal to another (see Guzei *et al.*, 2008).

Overlays made with the program *Mercury* (Macrae *et al.*, 2008) show that the structures at 100 K of the flash-cooled crystal and the slowly cooled crystal are indistinguishable, both in the positions of the atoms and the characteristics of the displacement ellipsoids. Furthermore, the occupancy factors for the one disordered lattice water O atom are the same [0.787 (14) versus 0.783 (7)]. It is therefore certain that the structure of the flashed-cooled crystal from which the first temperature sequence was started is the same as the structure of a crystal cooled slowly through the transition. The two crystals were, however, almost certainly imperfect in different ways and to different extents. Data from the slow-cooled crystal did give somewhat lower agreement factors, lower estimated uncertainties, and a flatter final difference map.

<sup>6</sup> Supplementary data for this paper are available from the IUCr electronic archives (Reference: HW5014). Services for accessing these data are described at the back of the journal.

Ellipsoid plots for the two crystallographically independent 15C5 molecules of the low-temperature phase at selected temperatures are shown in Fig. 7 for the crystal that was heated. Full ellipsoid plots for all structures determined during the heating sequence are included with the supplementary material. Viewing these 22 plots in succession produces a kind of movie of the asymmetric unit as a function of temperature. The orientation of these plots is the same as in Fig. 3(a).

## 4. Results

### 4.1. Overview of the structure

The structure is built from hydrogen-bonded chains along **a** of alternating 15C5 molecules and  $[\text{Ni}(\text{H}_2\text{O})_6]^{2+}$  cations (see Fig. 1); these chains are linked in the **b** and **c** directions by

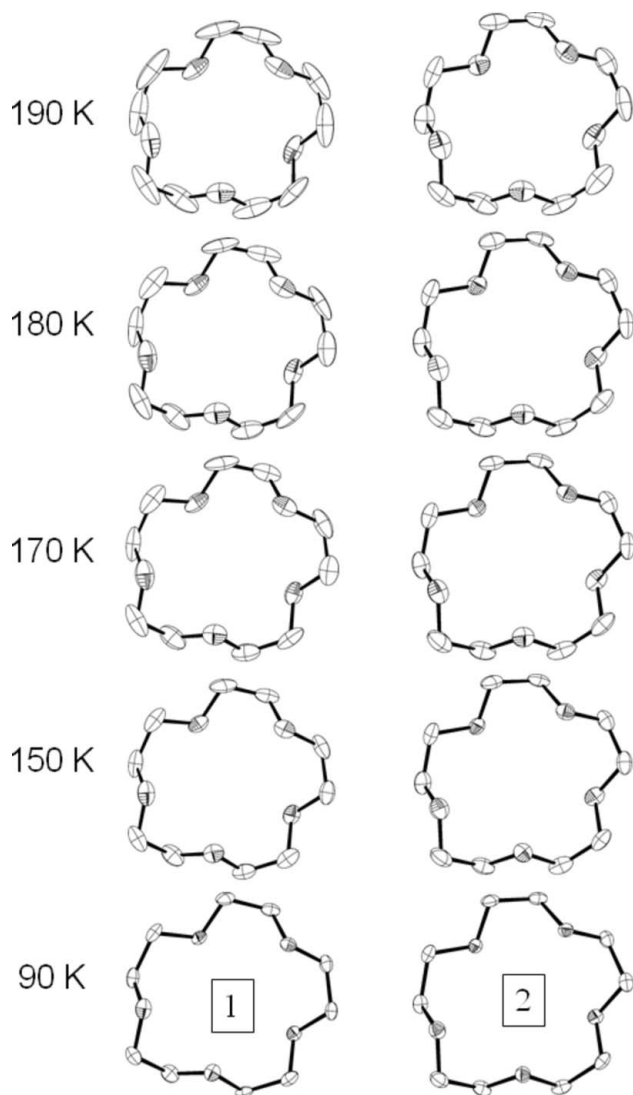


**Figure 7**  
Displacement parameters (50% probability level) for the atoms of the two crystallographically independent 15-crown-5 molecules of the low-temperature phase at selected temperatures.

corrugated sheets of hydrogen bonds involving the nitrate counterions and the lattice water molecule (see Fig. 2 and the supplementary material). These sheets are located at  $x = \frac{1}{2}$  in the high-temperature phase and at  $x = \frac{1}{4}$  and  $\frac{3}{4}$  in the low-temperature phase; the ridges and grooves are parallel to **c**. These hydrogen-bonded chains are a common feature in structures of metal complexes crystallized in the presence of 15C5 (Siegler *et al.*, 2010).

All 12 H atoms of the six water ligands are clearly involved in hydrogen bonds. Atoms O6 and O7, the ‘axial’ water ligands of the cations, form  $\text{O}-\text{H}\cdots\text{O}$  bonds to O atoms of adjacent 15C5 molecules; the ‘equatorial’ water ligand containing O8 forms an  $\text{O}-\text{H}\cdots\text{O}$  bond with the remaining 15C5 O atom (see Fig. 1). Six of the remaining seven H atoms of the water ligands make hydrogen bonds to nitrate O atoms; the seventh H atom (attached to O11) is donated to the lattice water molecule (O18). One of the H atoms attached to O18 is donated to the O atom (O13) of a nitrate ion, but it is not clear whether the other O18 H atom makes an hydrogen bond to O16, O17, both or neither (see Fig. 2). Each nitrate ion accepts four hydrogen bonds.

Most of the hydrogen-bonding  $\text{O}\cdots\text{O}$  distances are shorter than 2.85 Å, but those in which the lattice water is the donor are all rather long ( $> 2.90$  Å) and sometimes seem to be unusually long ( $> 3.00$  Å). If the  $\text{O}\cdots\text{O}$  distances only are considered then it seems that in the high-temperature structure the lattice water (O18) should be hydrogen-bonded to O13 and O16 of adjacent nitrate ions (see Fig. 2). That assignment, however, would require an impossibly small ( $< 80^\circ$ )  $\text{H}-\text{O}-\text{H}$  angle. Perhaps the bond is to O17, which is, however, 0.15–0.20 Å farther away from O18 than O16. The restrained refinement of the H-atom positions supports this latter interpretation. Another possibility is that the hydrogen bond is bifurcated.

Fits of the two independent 15C5 molecules of the low-temperature phase with each other and with the one molecule of the high-temperature phase were made with the program *XP-OFIT* (Sheldrick, 2008). The root-mean-square deviations were all less than 0.08 Å, which means that the conformations of the three 15C5 molecules are all the same.

### 4.2. Structural changes through the phase transition

The structures below and just above the transition were compared by making rotatable overlays of the packing using the program *Mercury* (Macrae *et al.*, 2008). A single overlay of all 11 (= 9 + 1 + 1) structures refined in the high-temperature cell shows that there is essentially no change in the average structure between 195 and 295 K. An overlay of the 9 (= 7 + 2) structures refined in the low-temperature cell in the range 90–150 K also shows nearly perfect overlap. An overlay of the 8 (= 6 + 2) low-temperature structures in the range 160–190 K, however, reveals that one of the independent 15C5 rings rotates slightly with *T* while the position and orientation with respect to the cell axes of the other ring are essentially constant. There are also small changes in the orientation of

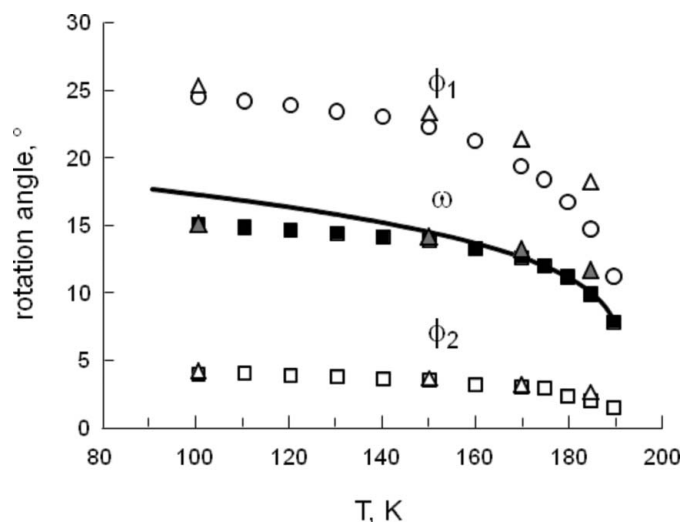


**Figure 8**  
Plot as a function of temperature of the rotation angle  $\omega$  relating the two independent 15C5 molecules in the low-temperature phase; the angle is for a rotation axis perpendicular to the average ring normal and approximately parallel to **a**. The uncertainties of the individual values are smaller than the symbols. Also shown are the dihedral angles between the least-squares planes of the nitrate ions:  $\phi_1$  for ions containing N1\_1 and N1\_2, and  $\phi_2$  for N2\_1 and N2\_2. The line is a fit of for a first-order transition function to  $\omega$  values for the heating sequence. Values for the four structures of the cooling sequence are shown as triangles.

one of the two nitrate ions containing N1. An overlay of the structures at 160 and 210 K is shown in Fig. 3.<sup>7</sup>

The rotation angle  $\omega$  needed to overlay the two independent 15C5 molecules of the low-temperature phase was calculated with the routine *AutoMolFit* in *PLATON* (Spek, 2003). The temperature dependence of this angle, which must go to zero at the transition to the high-temperature phase, is shown in Fig. 8; numerical data are available with the supplementary material. The rotation axis corresponding to the best overlap of the rings is approximately parallel to **a** and nearly perpendicular to **b**. The orientation of the rotation axis remains essentially constant with temperature (angles of this axis with **a**, **b** and **c** are 6.2–7.0, 89.3–90.3 and 96.1–96.9°).

The orientation of the nitrate ion containing N1\_1 also varies between 160 and 210 K (see the lower drawing in Fig. 9 or projections of the structure along **c**). The variation with  $T$  of the dihedral angle  $\phi_1$  between the least-squares planes of the nitrate ions containing N1\_1 and N1\_2 is shown in Fig. 8. The change in  $\phi_1$  is greater than the change in  $\omega$ , but the number of atoms affected is much smaller.

The angles  $\omega$  and  $\phi_1$  at *ca* 30–50 K below the phase transition are a little different for the crystal that was warmed through the transition than for the crystal that was cooled

through the transition (see Fig. 8). The differences are small but (especially in the case of  $\phi_1$ ) well beyond the estimated uncertainties. Overlays made with *Mercury* of the two structures (one from the heating sequence and one from the cooling sequence) at 185 K and at 170 K show that the differences at 185 K are real; each of the 10 pairs of C atoms in the 15C5 rings that do not quite overlap have the same relationship; one of the two rings is rotated relative to the crystal axes just slightly more than the other. The difference in the

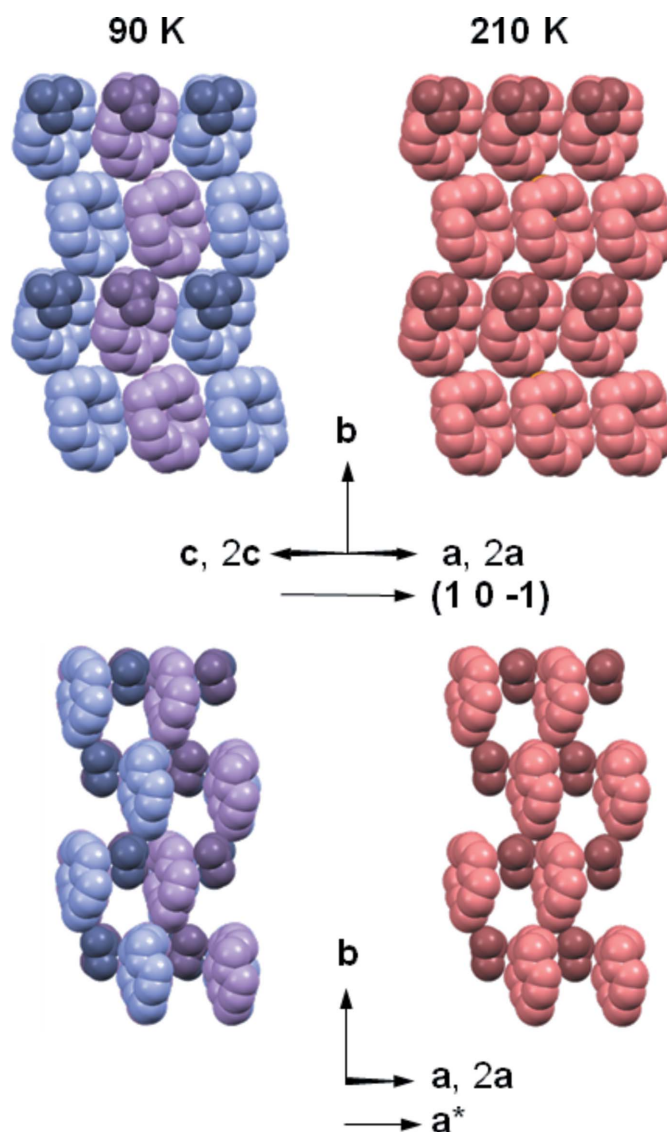


**Figure 9**  
Space-filling drawings showing the packing of the chemical units (the 15-crown-5 molecules and the nitrate ions containing N1) for which the changes in orientation through the phase transition are most obvious. The blue units in the low-temperature phase at 90 K have very nearly the same orientations as the red units at 210 K, but the blue and purple units of the 90 K structure have slightly different orientations. The upper and lower drawings are related by a rotation of *ca* 50° around the vertical [*i.e.* by the angle between (1 0  $\bar{1}$ ) and (1 0 0)]. The subtle differences between the 15-crown-5 orientations are more obvious in the upper drawing, particularly if spaces between the molecules are considered. The small differences between the orientations of the nitrate ions are more obvious in the lower drawing.

two nitrate ions (*i.e.* the difference in  $\varphi_1$ ) is also clear. At 170 K it is harder to find differences in the C-atom positions and thus in the ring rotations but a difference in the position of O14\_1 in the nitrate ion containing N1\_1 is still obvious.

There is a noticeable difference between the two phases in the disorder of the water molecules. In the high-temperature phase atom O18 of the lattice water molecule is obviously disordered (see Fig. 6); with occupancy factors for the major site in the range 0.66 (1)–0.73 (1). In the low-temperature phase O18\_1 is disordered [occupancy factors 0.68 (1)–0.79 (1)] but O18\_2 is better described as ordered.

All other differences between the two phases and between the two formula units in the low-temperature phase are very subtle, as is illustrated by the temperature dependence of the angle  $\varphi_2$  between the least-squares planes of the nitrate ions containing N2\_1 and N2\_2 (see Fig. 8).

### 4.3. Changes in displacement ellipsoids

The anisotropic displacement parameters show (see Fig. 7 and the supplementary material) that the structure is well ordered (except for one of the lattice water molecules) at 90 K and that the displacement ellipsoids expand with increasing temperature. The orientations of the ellipsoids indicate that the most important motions are librations of the 15C5 rings. Above *ca* 150 K the ellipsoids of ring 1 become progressively larger than those of ring 2. By 175–180 K the ring 1 ellipsoids are sufficiently elongated to suggest libration in a potential that is either very flat or that has two wells separated by a barrier small enough that disorder between them is dynamic. At 190 and 195 K the refined ellipsoids (see supplementary material) are very elongated because the smaller high-temperature cell is only an approximation. Since the high-temperature cell becomes a better description with increasing  $T$ , the ellipsoids shrink slightly as  $T$  is changed from 190 to 200 K.

### 4.4. Temperature of the phase transition

The DSC experiments, which used samples that had been ground into powders, indicate that one very small exotherm/endotherm pair occurs during a cooling/heating cycle. The hysteresis width is 2 (1) K (see Fig. 4); the average temperature is 191 (1) K. The peaks were too small to integrate reliably. The non-zero  $\Delta H^\circ$  values and the hysteresis indicate that the transition is first-order, but the very small heat change suggests a transition that is close to being continuous.

A plot of the sum of the intensities of the ten strongest  $h0\ell$ ,  $h$  and  $\ell = 2n + 1$ , reflections measured for the low-temperature phase during the heating sequence is shown in Fig. 10. Plots of the intensities of those individual reflections, which are systematically extinct in the high-temperature phase, are given with the supplementary material. Extrapolation of the intensities to zero suggests that the temperature of the transition is 195 (1) K when a single crystal is heated slowly.

A careful examination of the reconstructed reciprocal-lattice slices (examples given in Fig. 5) suggests that at 200 K there is still some scattering at the positions expected for  $h0\ell$ ,  $h$  and  $\ell = 2n + 1$ , reflections of the low-temperature phase, but that the scattering is very weak and somewhat diffuse. This observation indicates that the integrated intensities plotted in Fig. 10 likely include some contribution from the diffuse component, in which case the phase transition temperature obtained from the extrapolation is an overestimate.

An analysis (see below) of the evolution of the structural parameters  $\omega$  (rotation angle relating two independent 15C5 rings) and  $\varphi_1$  (dihedral angle between nitrate ions containing N1\_1 and N1\_2) as a function of  $T$  gives the transition temperature as 190–200 K, depending on the model used to fit the data and extrapolate the angles to zero.

The plots of cell constants with temperature are given in Figs. 11 and 12 for both the heating and the cooling sequences. The inflections between 190 and 200 K in the slopes of all the cell parameters measured in the more extensive heating sequence indicate that the transition occurs between these two temperatures. It appears that  $c$  is a little larger (0.007–0.013 Å above 160 K) for the crystal that was cooled through the transition.

It is clear that the apparent transition temperature found may depend on the method used to determine it and on the history and physical characteristics of the sample studied. In this case the powdered sample used in the DSC measurements appears to exhibit a slightly lower transition temperature than indicated by the evolution with heating of the cell constants and structural parameters determined from single-crystal data.

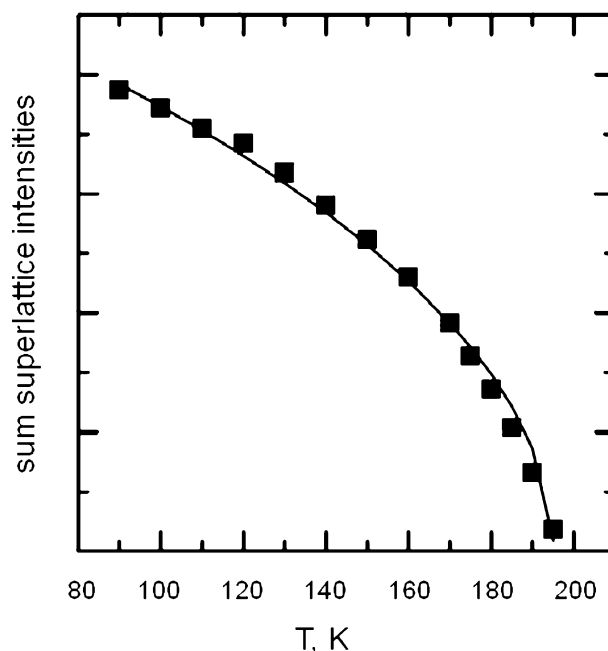


**Figure 10** Variation with temperature of the sum of the intensities of ten of the strongest  $h0\ell$ ,  $h$  and  $\ell$  odd, reflections of the low-temperature phase as measured for the heating sequence. The line is a power-law relationship  $I \propto (T_c - T)^{2\beta}$  with  $T_c = 195$  K and  $\beta = 0.27$ .

#### 4.5. Variation of the cell constants with temperature

The plots of the variation of the cell constants with  $T$  (Figs. 11 and 12) show that the changes between 90 and 273 K are larger for  $a$  (0.9%;  $a/2$  below 200 K) and  $b$  (1.1%) than for  $c$  (0.3%;  $c/2$  below 200 K). The curve for  $a$  is relatively smooth, but the curves for  $b$ ,  $c$  and  $\beta$  show obvious changes just below 200 K. The changes in the curvatures suggest a more rapid structural evolution in the range 170–195 K than for  $T < 170$  K, as does the plot (Fig. 8) of the  $\omega$  and  $\varphi_1$ . The DSC, however, shows no feature in the range 173–190 K.

Strain tensors for the heating sequence were calculated using an updated version of the program *STRAIN*, which was originally written by Ohashi and Finger and published in an

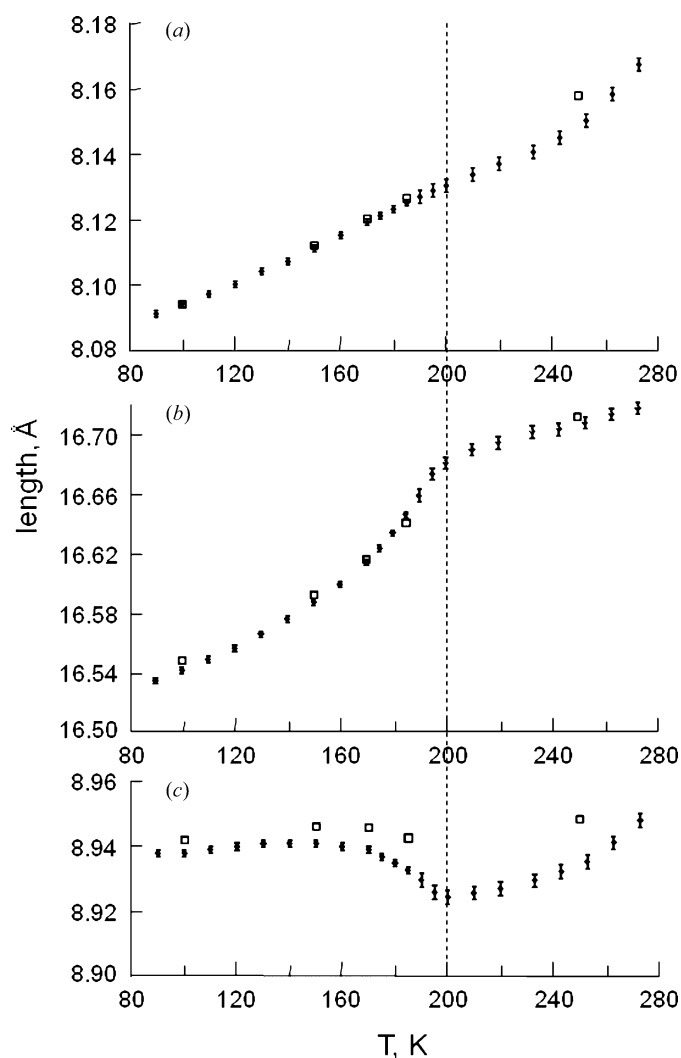


**Figure 11**

Variation with temperature of the cell constants  $a$ ,  $b$  and  $c$ . The values of  $a$  and  $c$  for the low-temperature phase have been halved to facilitate comparisons. The vertical scales have been chosen so that the fractional change per unit is similar in the three drawings. The lengths of the error bars, which are shown for the 22 structures of the heating sequence, are twice the precision of the cell constant determination. Cell constants for the five structures of the cooling sequence are shown as open squares. The vertical dashed line marks the upper limit of the phase transition temperature.

appendix in Hazen & Finger (1982). One principal axis of the thermal expansion tensor is necessarily parallel to  $\mathbf{b}$ ; a second is close to  $\mathbf{c}$  (average angular deviation  $11.3^\circ$ ; range  $4.1$ – $20.0^\circ$ ). Owing to the good alignment of the principal axes of the expansion tensor and the cell axes the plots of the cell constants *versus*  $T$  are good representations of the thermal expansion.

#### 4.6. Interpretation in terms of mean-field theory

The concept of a structural phase transition provides a way in which to interpret the different types of measurable parameters (structural distortion, superlattice intensities and changes in cell parameters) that can be used to follow the evolution of the low-symmetry phase up to the phase transition. Mean-field theories (such as that developed by Landau; see Landau & Lifshitz, 1969; Toledano & Toledano, 1987) provide precise symmetry-constrained relationships between these quantities and show how they can be represented in terms of an ‘order parameter’ denoted as  $Q$ . These relationships have been shown to hold in a wide variety of structural phase transitions and in a wide variety of crystalline materials. Here we explore whether such relationships hold for the transition in NiW6-W. Full analyses were carried out for the

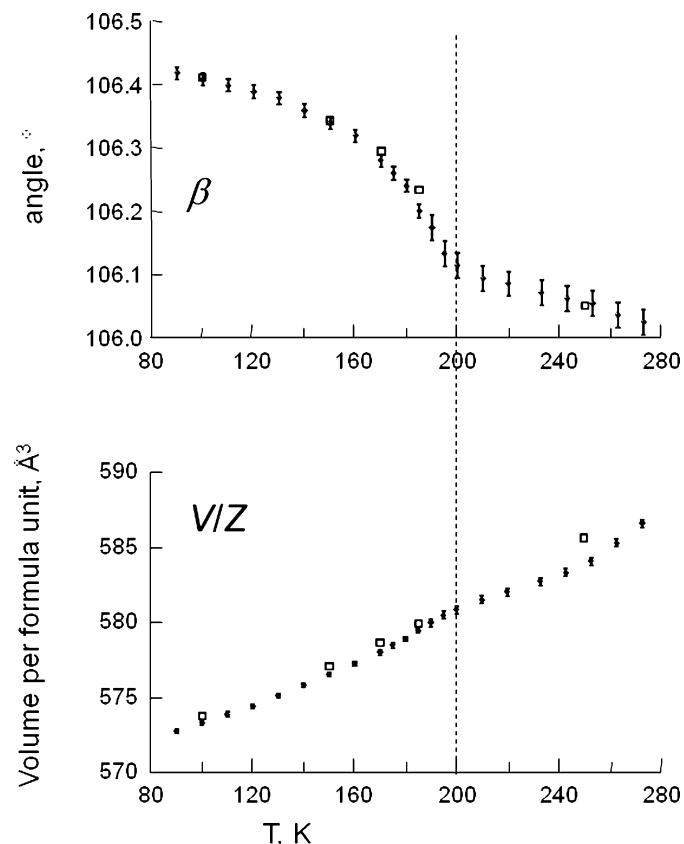


**Figure 12**

Variation with temperature of the cell volume per formula unit ( $V/Z$ ) and the cell constant  $\beta$ . The lengths of the error bars, which are shown for the 22 structures of the heating sequence, are twice the precision of the cell constant determination. Cell constants for the five structures of the cooling sequence are shown as open squares. The vertical dashed line marks the upper limit of the phase transition temperature.

heating sequence only but we see no indication that an analysis for a cooling sequence would lead to a different conclusion.

**4.6.1. Structural order parameters.** The major evolution within the lower-symmetry structure is the change of the relative rotation angle ( $\omega$ ) between the two 15C5 rings that are related by symmetry above the phase transition, and the change in the relative orientation ( $\phi_1$ ) of the nitrate anions containing N1\_1 and N1\_2 (see Fig. 8). The value of  $\phi_1$  varies nearly linearly with  $\omega$  (Fig. 13) and so reflects the same underlying process of structural evolution. We have therefore associated the  $\omega$  rotation angle with the primary order parameter. At first glance Fig. 8 then appears to show classic first-order behavior of the order parameter, with a steady decrease in  $\omega$  with increasing  $T$  as the phase transition is approached from below, followed by an abrupt drop to zero at the transition. This behavior would be consistent with the observation of a small peak in the DSC data which also indicates a first-order transition. In Landau mean-field theory, the evolution of the order parameter below a first-order phase transition at  $T_{tr}$  is given by

$$Q^2 = \frac{2}{3} Q_0^2 \left[ 1 + \left[ 1 - \frac{3}{4} \left( \frac{T - T_c}{T_{tr} - T_c} \right) \right]^{1/2} \right]. \quad (2)$$

The jump in the order parameter at the transition temperature  $T_{tr}$  is  $Q_0$ . A fit of this equation to the values of  $\omega$  immediately below the transition yields a transition temperature  $T_{tr} = 191$  K, consistent with the DSC data, and a jump in  $\omega$  from 0 to  $6.8^\circ$  at the transition. However, extrapolation of this fit to lower temperatures predicts larger rotation angles  $\omega$  than are observed (see Fig. 8).

This sort of deviation from the Landau equation is commonly observed in mineral transformations at low temperatures and is commonly attributed to ‘order parameter

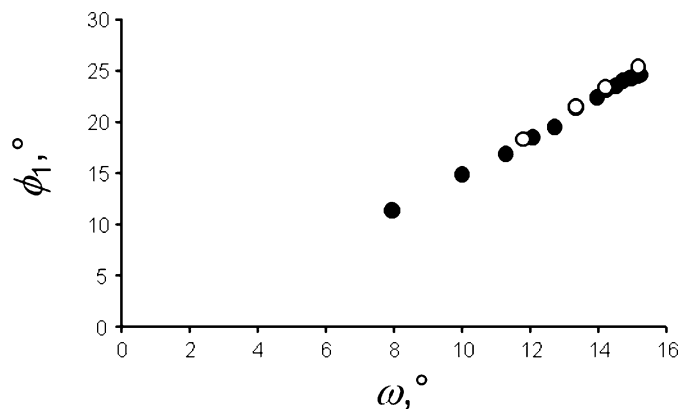


**Figure 13**

The relationship of the two structural parameters that change most in the low-temperature phase (see text). The dihedral angle  $\phi_1$  between the least-squares planes of the nitrate ions containing N1\_1 and N1\_2 varies nearly linearly with the rotation angle  $\omega$  relating the two independent 15C5 molecules in the low-temperature phase. Note that  $\omega$  and  $\phi_1$  increase as the temperature decreases so that the points corresponding to the lowest temperatures are at the upper right of the plot. Values for the four structures of the cooling sequence are shown as open circles.

saturation’ as a consequence of quantum mechanical effects (Salje, Wruck & Thomas, 1991; Salje, Wruck & Marais, 1991; Perez-Mato & Salje, 2000, 2001) at low temperatures. The general formulation for the evolution of the order parameter under the influence of saturation then becomes

$$Q^n = \Theta_s \left[ \coth \left( \frac{\Theta_s}{T_c} \right) - \coth \left( \frac{\Theta_s}{T} \right) \right] \quad (3)$$

with  $n = 2$  for a second-order transition and  $n = 4$  for a tricritical transition. The effect of saturation is modeled with a ‘saturation temperature’  $T_s$ . A second order and a tricritical expression fit the evolution of the  $\omega$  angle equally well, and far better than a first-order fit without saturation (Fig. 8), thus indicating that the apparent order of the transition cannot be unequivocally determined from these data. However, while such saturation may play a role in this transition, the fits yield values for the saturation temperature of  $T_s > 450$  K, which seems unreasonably high for a molecular solid. Therefore, it seems unlikely that the transition can be described by the evolution of a single order parameter.

**4.6.2. Intensities of superlattice reflections.** The transition involves the doubling of the unit-cell parameters  $a$  and  $c$  of the high-temperature  $P2_1$  phase and the development of a  $B$ -lattice in the low-temperature phase. It is thus a zone-boundary transition, with a critical point  $(\frac{1}{2}, 0, \frac{1}{2})$  in the Brillouin zone of the high-temperature phase, which accounts for the appearance of the super-lattice reflections with  $h, \ell$  both *odd* (to satisfy the  $B$ -lattice condition) within the low-symmetry phase. The intensities of the superlattice reflections should therefore evolve linearly with the square of the order parameter,  $I(h, \ell = \text{odd}) \propto Q^2$  and the evolution of the superlattice intensities gives an additional way in which to follow the structural evolution.

However, while the sum of the strongest  $h0\ell$  intensities follows this relation down to *ca* 170 K, there is a significant deviation from linearity at lower temperatures (Fig. 14), while the evolution of the intensities with temperature follows a smooth power law (Fig. 10). The deviation between the intensities and the structural order parameter cannot be a result of order-parameter saturation because that only affects the variations with temperature of the order parameter (as well as coupled quantities), and does not change the proportionality of the intensities with  $Q$ . The plot of intensity against  $Q$  therefore suggests that a second process is involved and that the phase transition and its evolution are not adequately described by a single order parameter.

**4.6.3. Cell constants and spontaneous strain.** The changes in the unit-cell parameters can be considered as the strain that arises spontaneously as a consequence of the transition, and provide a further method by which to follow the transition and determine its thermodynamic character. The spontaneous strain is a second-rank tensor having six independent components  $e^{ij}$  (Carpenter *et al.*, 1998). In order to determine the components of the spontaneous strain, the cell parameters of the high-temperature phase have to be extrapolated below the transition to the temperatures at which the cell parameters were measured for the low-symmetry phase. This extrapola-

tion eliminates the intrinsic effects of thermal expansion from the spontaneous strain, but introduces considerable uncertainties in the results. The unit-cell parameters and volume in the high-symmetry phase show significant curvature and were fit with an equation of the form

$$y = y_1 + y_2\theta \coth(\theta/T) \quad (4)$$

on the assumption that the curvature is due to low-temperature saturation (Salje, Wruck & Thomas, 1991). The behavior of the cell volume above  $T_c$  yielded unexpected parameters;  $\theta$  is expected to be *ca* 100 K for a molecular crystal, but the fitted value was 665 K, which is very high even for a crystal like this one that is partially ionic. However, lower and more 'reasonable' values of the saturation temperature do not allow the volume data above the transition to be fit, and give unphysical values for the volume strain below the transition. These results may indicate that the curvature in the unit-cell parameters of the high-temperature phase is due instead to anharmonic effects. Whatever the physical cause, this cannot be determined with the limited range of data for the high-temperature phase. The critical requirement is that the function used to fit the cell parameters of the high-temperature phase provide physically reasonable descriptions of their variation in the high-temperature phase and their extrapolation to below the transition. Therefore the remaining cell parameters were fit and extrapolated with the assumption that  $\theta = 665$  K.

The resulting components of the spontaneous strain all suggest that the transition is continuous, although small first-order steps at the transition cannot be excluded. The different strain components, however, do not all vary with temperature in the same way. The volume strain and the component  $e^{11}$  are linear (indicative of a second-order transition) while  $e^{33}$  and

$e^{13}$  evolve approximately quadratically; details are given in the supplementary material. The largest component  $e^{22}$ , which is the compression of **b**, varies approximately linearly near  $T_c$  but not at larger values of  $(T_c - T)$ . This variety of evolution of the strains with  $(T_c - T)$  is similar to the variety in the variation of the superlattice intensities. Furthermore, for transitions such as this, without a change in crystal system, all of the components of the spontaneous strain are non-symmetry breaking and should thus be proportional to the square of the driving order parameter and thus linear with the superlattice intensities:  $e_i \propto V_S \propto I(h, l = \text{odd}) \propto Q^2$ . However, this linearity is only observed within 30 K of the phase transition, as is also the case for the superlattice intensities (Fig. 14).

## 5. Discussion

Initially we thought that the phase change in this system must be a simple order–disorder transition. The constancy between room temperature and 200 K of the tangential component of the ellipsoids of the 15C5 ring strongly suggested that the ring libration is governed by a double-well potential so that the ring should be considered to be dynamically disordered. The transition changes the size of the asymmetric unit but if a correction is made for the doubling of *a* and *c* there is no discontinuity in the cell constants. The heat change at the transition is almost too small to observe. The transition itself appears to be continuous, or very close to being so; the crystal continues to diffract well as it passes through the transition at 190–200 K. At 90 K the structure, except for the O atom of one of the lattice water molecules, is ordered and all the displacement ellipsoids are small and regular.

There is, however, an important problem with this simple description: the atoms of the 15C5 ring in the high-temperature structure are not at positions that are averages of the two sets of positions in the low-temperature structure. Structure overlays show that ring 2 of the low-temperature form is nearly coincident with the high-temperature ring while ring 1 of the low-temperature form is not. When the crystal is cooled the rotation of ring 1 away from ring 2 starts at *ca* 200 K and continues until *ca* 160 K. The transition therefore cannot correspond to a simple ordering in the two wells of a double-well potential similar to that found above 200 K. The potential energy surface must change through the transition.

Recent tests of crystal-structure prediction for molecular compounds (see Dunitz *et al.*, 2000; Motherwell *et al.*, 2002; Day *et al.*, 2005, 2009; van Eijck, 2005) have shown that there are large numbers of potential-energy minima that differ by only a few  $\text{kJ mol}^{-1}$  and that corresponds to structures that differ in very subtle ways. The complexity of such energy surfaces is usually a consequence of the complicated shapes of most molecules, of their conformational flexibility and of their relatively weak intermolecular interactions; the energy surfaces for compounds of smaller ions, which have simpler shapes and are less flexible, and those of extended frameworks are expected to have fewer features. It may then be unreasonable to expect a phase transition in a molecular crystal to

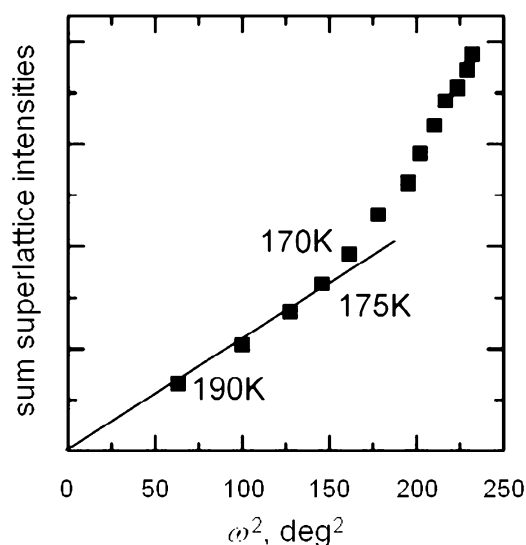


**Figure 14**

The variation as measured for the heating sequence of the sum of the intensities of ten of the strongest  $h0\ell$ ,  $h$  and  $\ell$  odd, reflections of the low-temperature phase with the square of the rotation angle that relates the orientations of the two 15C5 rings. Lines are drawn as guides to the eye to emphasize the different evolution above and below 170 K.

be simple. The minima of the energy surface are so close to each other and so similar in energy that a change in temperature, and therefore in vibrational and librational amplitudes, can influence not only the populations but also the positions and relative depths of the minima. The change with  $\omega^2$  of the intensities of the superlattice reflections (Fig. 14) and the change with  $T$  of  $c$  (Fig. 11) support the idea that the potential energy surface below the transition is not simple.

There are small differences just below the transition between the crystal that was flash-cooled and then heated and the crystal that was cooled slowly. We cannot say whether these differences are a result of having used two crystals with different types, patterns and frequencies of defects, or the result of a difference between heating and cooling, but the former explanation seems more probable. In any event the differences are too small to affect the conclusions drawn; in both cases one 15C5 ring rotates but the other does not. It would be much more normal for the average structure of the low-temperature phase to change little with  $T$  while the portions of the structure no longer related by the symmetry evolve equally and in opposite directions.

This study also points out that the structural changes with  $T$  within a phase can be comparable to, or even larger than, the changes between phases that can be distinguished easily by crystallographic methods.<sup>8</sup> Changes in the cell constants with  $T$ , and especially changes in  $c$ , are by no means confined to the region where the superlattice reflections appear or disappear and where the DSC shows an endo- or exotherm. Such changes outside the region of a phase transition, which have sometimes been described as ‘premonitory behavior’, may be evidence of a complicated potential-energy surface but are entirely analogous to the behavior of inorganic compounds approaching structural phase transitions to higher-symmetry phases.

## 6. Summary

A detailed study of the phase transition of the first polymorph of  $[\text{Ni}(\text{H}_2\text{O})_6](\text{NO}_3)_2 \cdot (15\text{-crown-5}) \cdot \text{H}_2\text{O}$  shows that important structural changes extend over a wide temperature range (*ca* 150–210 K), although the transition temperature, as measured by DSC and by the changes in reflection conditions, is clearly near the upper end of this range.

While the transition is almost surely related to the thermal contraction, we could identify no simple reason for the transition; the changes in the structure through the transition are just too subtle. There are no intramolecular (or interionic) contacts at 200 K short enough to suggest that a transition with cooling is imminent. Changes in the hydrogen bonds formed by the lattice water molecules may be important in driving the transition, but in the absence of a neutron diffraction study it is impossible to know.

<sup>8</sup> This is always strictly true at a continuous phase transition, at which there is only an infinitesimal difference in the structures of the two phases at the equilibrium transition temperature.

The largest structural changes are in the orientations of half of the 15C5 molecules and one quarter of the nitrate ions of the high-temperature phase. All the nitrate ions containing N1 are in contact with two (or possibly three) 15C5 molecules in slabs containing the planes  $\{1\ 0\ \bar{1}\}$ . Below the transition the 15C5 molecules and N1 nitrate ions in every other slab have undergone a small reorientation. As the nitrate ions interact with several 15C5 rings it seems that the transition must be cooperative. Since layers alternate in the direction  $[1\ 0\ \bar{1}]^9$  (see Fig. 9) it seems likely that the change in half of the layers allows the layers to fit together more tightly.

The transition cannot be described in terms of a Landau-type free-energy expansion with a single order parameter, probably because the free-energy surface of this basically molecular solid is more complex than those involved in transitions in many inorganic framework structures, for which the theory is known to be a good description. The structural connectivity of a framework solid can act to propagate elastic fields that act as a mean field and simplify the energy surface, whereas in a molecular crystal the forces are weaker and act over shorter distances. The higher symmetry of most inorganic framework structures compared with molecular solids may also be a factor. It is not possible, however, to make a general statement about the applicability of mean-field theory to phase transitions in molecular crystals until more studies of the detailed evolution of the structure, cell parameters and super-lattice intensities below phase transitions have been made. Such studies are a sensitive probe of the complexity of the energy surface.

MAS thanks the University of Kentucky for a 2006–2007 Kentucky Opportunity Fellowship. We also thank Clare Macrae of the CCDC for her help with the program *Mercury*.

## References

- Allen, F. H. (2002). *Acta Cryst.* **B58**, 380–388.  
 Angel, R. J. (1992). *Am. Mineral.* **77**, 923–929.  
 Arlt, T. & Angel, R. J. (2000). *Phys. Chem. Miner.* **27**, 719–731.  
 Budzianowski, A., Katrusiak, A. & Szafranski, M. (2008). *J. Phys. Chem. B*, **112**, 16619–16625.  
 Carpenter, M. A. (2007). *Am. Mineral.* **92**, 309–327.  
 Carpenter, M. A., Becerro, A. I. & Seifert, F. (2001). *Am. Mineral.* **86**, 348–363.  
 Carpenter, M. A., Salje, E. K. H. & Graeme-Barber, A. (1998). *Eur. J. Mineral.* **10**, 621–691.  
 Casati, N., Macchi, P. & Sironi, A. (2009). *Chem. Eur. J.* **15**, 4446–4457.  
 Chernyshov, D., Hostettler, M., Törnroos, K. W. & Bürgi, H. B. (2003). *Angew. Chem. Int. Ed. Engl.* **42**, 3825–3830.  
 David, W. I. F., Ibberson, R. M., Cox, S. F. J. & Wood, P. T. (2006). *Acta Cryst.* **B62**, 953–959.  
 Day, G. M. *et al.* (2005). *Acta Cryst.* **B61**, 511–527.  
 Day, G. M. *et al.* (2009). *Acta Cryst.* **B65**, 107–125.  
 Dunitz, J. D., Filippini, G. & Gavezzotti, A. (2000). *Helv. Chim. Acta*, **83**, 2317–2335.  
 Eijck, B. P. van (2005). *Acta Cryst.* **B61**, 528–535.  
 Flack, H. D. (1983). *Acta Cryst.* **A39**, 876–881.

<sup>9</sup> The angle between  $[1\ 0\ \bar{1}]$  and  $(1\ 0\ \bar{1})$  is  $5.6^\circ$  at 190 K.

- Flack, H. D. & Bernardinelli, G. (2000). *J. Appl. Cryst.* **33**, 1143–1148.
- Goeta, A. E., Howard, J. A. K., Hughes, A. K., O'Hare, D. & Copley, R. C. B. (2007). *J. Mater. Chem.* **17**, 485–492.
- Guzei, I. A., Bikzhanova, G. A., Spencer, L. C., Timofeeva, T. V., Kinnibrugh, T. L. & Campana, C. F. (2008). *Cryst. Growth Des.* **8**, 2411–2418.
- Haddon, R. C., Sarkar, A., Pal, S. K., Chi, X., Itkis, M. E. & Tham, F. S. (2008). *J. Am. Chem. Soc.* **130**, 13683–13690.
- Hashizume, D., Miki, N., Yamazaki, T., Aoyagi, Y., Arisato, T., Uchiyama, H., Endo, T., Yasui, M. & Iwasaki, F. (2003). *Acta Cryst.* **B59**, 404–415.
- Hazen, R. M. & Finger, L. W. (1982). *Comparative Crystal Chemistry*. New York: Wiley.
- Herbstein, F. H. (2006). *Acta Cryst.* **B62**, 341–383.
- Howard, C. J. & Stokes, H. T. (2005). *Acta Cryst.* **A61**, 93–111.
- Landau, L. D. & Lifshitz, E. M. (1969). *Statistical Physics*. Oxford: Pergamon Press.
- Macrae, C. F., Bruno, I. J., Chisholm, J. A., Edgington, P. R., McCabe, P., Pidcock, E., Rodriguez-Monge, L., Taylor, R., van de Streek, J. & Wood, P. A. (2008). *J. Appl. Cryst.* **41**, 466–470.
- Minkov, V. S., Tumanov, N. A., Kolesov, B. A., Boldyreva, E. V. & Bizyaev, S. N. (2009). *J. Phys. Chem. B*, **113**, 5262–5272.
- Motherwell, W. D. S. *et al.* (2002). *Acta Cryst.* **B58**, 647–661.
- Nichol, G. S. & Clegg, W. (2005). *Acta Cryst.* **B61**, 464–472.
- Nonius (2000). *COLLECT*. Nonius BV, Delft, The Netherlands.
- Otwinowski, Z. & Minor, W. (2006). *International Tables for Crystallography*, Vol. F, 1st online ed., ch. 11.4, pp. 226–235. Chester: International Union of Crystallography.
- Ovcharenko, V. I., Romanenko, G. V., Maryunina, K. Y., Bogomyakov, A. S. & Gorelik, E. V. (2008). *Inorg. Chem.* **47**, 9537–9552.
- Perez-Mato, J. M., Orobengoa, D. & Aroyo, M. I. (2010). *Acta Cryst.* **A66**, 558–590.
- Perez-Mato, J. M. & Salje, E. K. H. (2000). *J. Phys. Condens. Matter*, **12**, L29–L34.
- Perez-Mato, J. M. & Salje, E. K. H. (2001). *Philos. Mag. Lett.* **81**, 885–891.
- Salje, E. K. H., Wruck, B. & Marais, S. (1991). *Ferroelectrics*, **124**, 185–188.
- Salje, E. K. H., Wruck, B. & Thomas, H. (1991). *Z. Phys. B Condens. Matter*, **82**, 399–404.
- Seredyuk, M., Gaspar, A. B., Kusz, J., Bednarek, G. & Gütlich, P. (2007). *J. Appl. Cryst.* **40**, 1135–1145.
- Sheldrick, G. M. (2008). *Acta Cryst.* **A64**, 112–122.
- Siegler, M. A. (2007). PhD Dissertation. University of Kentucky.
- Siegler, M. A., Parkin, S., Selegue, J. P. & Brock, C. P. (2008). *Acta Cryst.* **B64**, 725–737.
- Siegler, M. A., Prewitt, J. H., Kelley, S. P., Parkin, S., Selegue, J. P. & Brock, C. P. (2010). *Acta Cryst.* **B66**, 213–221.
- Spek, A. L. (2003). *J. Appl. Cryst.* **36**, 7–13.
- Törnroos, K. W., Hostettler, M., Chernyshov, D., Vangdal, B. & Bürgi, H.-B. (2006). *Chem. Eur. J.* **12**, 6207–6215.
- Toledano, J. C. & Toledano, P. (1987). *The Landau Theory of Phase Transitions*. Singapore: World Scientific.
- Tribaudino, M., Nestola, F., Cámara, F. & Domeneghetti, M. C. (2002). *Am. Mineral.* **87**, 648–657.
- Tribaudino, M., Nestola, F., Meneghini, C. & Bromiley, G. D. (2003). *Phys. Chem. Miner.* **30**, 527–535.